An Adsorption Reverse Electrodialysis system for the generation of electricity from low-grade heat

An Adsorption Reverse Electrodialysis system for the generation of electricity from low-grade heat

C. Olkis[a], G. Santori[a]* and S. Brandani[a]

[a] *The University of Edinburgh, School of Engineering, Institute for Materials and Processes, Sanderson Building, The King's Buildings, Mayfield Road, EH9 3JL Edinburgh, Scotland, UK*

*Corresponding author: G.Santori@ed.ac.uk

Abstract

A novel process is presented to generate electricity from low-grade heat by combining a Reverse Electrodialysis membrane with an Adsorption desalinator in a closed-loop system. A Reverse Electrodialysis membrane generates electricity by controlled mixing of two salt solutions of different concentrations. An Adsorption desalinator restores the initial salt gradient by utilising low-grade heat for the separation. In this study the process is designed from optimising the salt and material selection to the development of the real system application. Energy and exergy efficiencies of the proposed system show the potential of this novel renewable energy technology. The efficiencies of 227 salts with a range of different valences and 10 adsorption materials have been investigated over a large number of system parameters. The results show that the optimised system can achieve an exergy efficiency of up to 30 %. Moreover, high salt concentrations do not significantly increase the specific energy consumption of the Adsorption desalinator, which allows operating the Reverse Electrodialysis membrane at the optimal salt concentrations.

Keywords: Adsorption desalination, Reverse Electrodialysis, Pitzer correlations, Gibbs free energy, closed-loop

---

1. Introduction

Climate change, water scarcity and energy security are some of the world's major issues. It is widely recognized that a key role in solving these issues is a sustainable and efficient use of the planet's limited resources. However, energy is not used efficiently, with estimates showing that 72 % of the global primary energy produced is converted to waste heat [1, 2].Low-grade heat available from numerous sources such as industrial sites, power plants, geothermal areas or solar collectors [3, 4].

Papapetrou et al. analysed the availability of industrial waste heat in the EU and estimated the availability at 300 TWh per year excluding power plants and transportation [5]. They categorised waste heat at different temperature levels between ambient temperature up to 1000 °C, where the highest waste heat potential lies below 200 °C representing one third of the emitted waste heat. Rattner and Garimella evaluated the waste heat potential in the USA in a comprehensive study including power plants, transportation and manufacturing [6]. They found that

4000 TWh of waste heat are annually available from condensers of power plants in the temperature range from 40-49 °C. Another 4500 TWh per year are emitted at temperature levels between 50-99 °C. Both temperature ranges amount to a total of 78 % of the entire waste heat available below 100 °C.

Recently, the utilisation of low-grade heat has attracted much attention, but only few of the proposed systems are able to operate at temperatures below 100 °C. The Organic Rankine Cycle (ORC) usually utilises waste heat between 100-300 °C [7]. Although, ORC systems operating between 80-100 °C have been proposed in simulations, which achieved exergy efficiencies of 54 % using highly toxic refrigerant R123 [8].
Thermoelectric systems are solid state power generators built of semiconductors that can generate electricity from a temperature difference, where any source of heat above ambient temperature can be used [9]. However, their efficiencies have been too low to be used in commercial applications [10] achieving exergy efficiencies of 10 % [9].
Another system utilising waste heat between 50-100 °C are Osmotic Heat Engines (OHE), which combine pressure retarded osmosis PRO with membrane distillation MD [11]. PRO membranes are semi-permeable, they convert the energy potential between salinity gradients into pressure first and then into electricity [12]. The salinity gradient is then restored by the MD unit in a closed-loop system. Lin et al. estimated the maximum thermodynamic limit of an OHE at an exergy efficiency of 81 %, which is a theoretical value neglecting all limitations of a real system [13].
However, none of these technologies have demonstrated the conversion of low-grade heat below 100 °C to electricity at efficiencies and costs sufficient to generate commercial interest [7].
Reverse Electrodialysis (RED) membranes are semi-permeable like PRO membranes, but RED is an electrochemical process directly converting the energy potential of the salinity gradients into electricity [12]. In 1977, Wick estimated the global potential of natural salinity gradients for the utilisation by either RED or PRO at 2.6 TW (≈ 22800 TWh/year) [14]. Recently, Veerman et al. have experimentally explored the generation of electricity by RED from naturally occurring salt gradients between river water and seawater. [15]. Experimental work has demonstrated that the electric power output of the RED membrane can be further improved by using concentrated brines from seawater brine basins [16]. However, naturally occurring salt gradients are relatively small, their availability is geographically limited and they cause membrane fouling, which reduces the membrane performance by 40 % without pre-treatment of the feed water [17].

The closed-loop system of salinity solutions overcomes these issues and the salinity gradient is restored by a thermal regeneration system as illustrated by Logan and Elimelech [18]. The general schematic of RED in a closed-loop system is shown in Fig. 1. The RED membrane generates electricity through the salt gradient of two feed solutions where one has a low and the other a high salinity. After flowing through the membrane, the thermal desalination unit utilises low-grade heat to regenerate the two solutions to their initial salt concentrations. The optimal performance of the system is a trade-off between the electricity generation and energy requirements for the separation process.

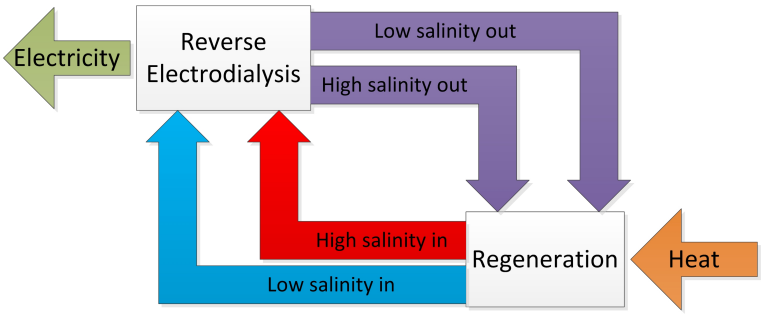

Figure 1: A simplified representation of the closed-loop system converting low-grade heat into electricity

The most common thermal desalination technology is multi effect distillation (MED), which has the highest efficiency among all thermal desalination technologies [19]. However, MED systems are very large as their efficiency improves with the number of stages and higher waste heat temperature [20], where their specific thermal energy consumption can be as low as 40 kWh/m^3 using 90 °C heat source temperature [7]. In addition, a MED plant requires an electrical input of 2.0-2.5 kWh/m^3 [21]. The number of stages and therefore the efficiency is limited at high salt concentrations.
Smaller desalination systems include membrane distillation MD, which can utilise low-grade heat 45-85 °C, but the thermal energy consumption varies widely for seawater from 200 to 6000 kWh/m^3 [22]. In addition, Zaragoza et al. reported a specific electric consumption of 20 kWh/m^3 [22].
MED and MD are a well established commercial thermal desalination techniques, while other emerging techniques include temperature swing adsorption systems [23]. Wu et al. introduced the thermodynamic specific energy consumption in adsorption desalination [24], which ranges between 700 to 1000 kWh/m^3. However, the electric energy consumption is only 1.4 kWh/m^3 [25]. Heat source temperatures used for adsorption desalination are usually 50-85 °C [25].

Any thermal desalination method can be coupled with RED in a closed-loop system to generate electricity from low-grade heat. A closed-loop system of an MED-RED plant was modelled by Tamburini et al. presenting exergy efficiencies of up to 30 %, which could be increased to 85 % by future optimising the membranes [7]. The proposed RED-MED system would utilise a low-grade heat source at 90 °C.
Adsorption desalinators can utilise low-grade heat sources between 50 to 85 °C and the development of new adsorption materials could reduce the regeneration temperature down to 40 °C. This would even allow their application in the afore-mentioned temperature window 40-49 °C, where vast quantities of waste heat are available from power plants. At the moment no technology can convert heat in this temperature range. Moreover, the internal electricity consumption of an AD plant is 50 % lower than MED, which improves the efficiency of the RED membrane. The very low heat source temperature, low electricity consumption, process simplicity and small system size [26] make adsorption desalination an ideal candidate for the integration into a closed-loop system combined with a RED membrane to convert low-grade heat into electricity. No work has been previously published on the utilisation of adsorption desalination in the closed-loop system.

The present study introduces this unprecedented process to generate electricity from low-grade heat by combining an adsorption desalinator with a Reverse Electrodialysis membrane. Striking features of the proposed Adsorption Reverse Electrodialysis (ADRED) system include a simple process design, a lower internal electricity consumption and the utilisation of low-grade heat sources below 70 °C.

The purpose of this study is the introduction and design of an ADRED system including the optimisation of the salt and adsorption material combination, performance analysis and process development.

The amount of electricity that can be generated in a RED membrane has been estimated by the Gibbs free energy of mixing ΔG_{mix} [27, 28]. On the regeneration side, the energy required to regenerate the salt solutions to the initial concentrations has been assessed by the specific energy consumption per unit of water (SEC) [24]. The ratio of ΔG_{mix} to the SEC determines the performance of the system. This included 227 salts, 10 different adsorption materials and different system parameters to optimise the combination to achieve the maximum ratio of ΔG_{mix} to the SEC. Further investigations determined the impact of the salt on the SEC and the thermodynamic adsorption cycle, which has a crucial aspect not been published. Finally, the process was assessed for a real system application, where pumping losses and the footprint of an exemplary plant with 200 kW electrical output were examined.

2. Methodology

2.1. The ADRED system

The main energy input into the system comes from a low-grade heat source converted into electricity as system output [5]. For ADRED, low-grade heat temperatures below 70 °C are of particular interest. Papapetrou et al. identify the main industries emitting waste heat below 100 °C as the food industry and the paper industry [5]. For example, the exhaust air from the drying section of a mid-sized paper machine has a temperature of 70 °C with a heat output of 6 MW [29]. Another possible heat source could be provided by a solar collector [30, 31]. The system could also utilise waste heat from power plants, which is available in very large quantities below 100 °C [6].

The flow scheme of the ADRED system can be seen in Fig. 2. The two main components of the ADRED system are the Reverse Electrodialysis membrane and the adsorption desalinator. The outlet of the high salinity solution is connected to the evaporator of the adsorption regeneration, where the solution is regenerated to its initial salt concentration. A part of the water is evaporated from the brine and the pure water vapour is adsorbed on the adsorption material. Low-grade waste heat is required to desorb the vapour from the material. Each adsorber undergoes a temperature swing adsorption cycle. The adsorption cycle includes a heating phase, when the adsorbate desorbs from the surface of the adsorbent material. Afterwards the material is cooled to ambient temperature to adsorb new adsorbate onto its surface. Therefore, one adsorption bed would only allow an intermittent process, since one bed can only either adsorb or desorb at a given time. Whereas, the addition of a second bed enables a semi-continuous

operation. In this case one bed can adsorb water from the evaporator, while the other bed desorbs water vapour. The desorbing vapour is condensed and mixed with the low salinity outlet solution coming from the membrane.

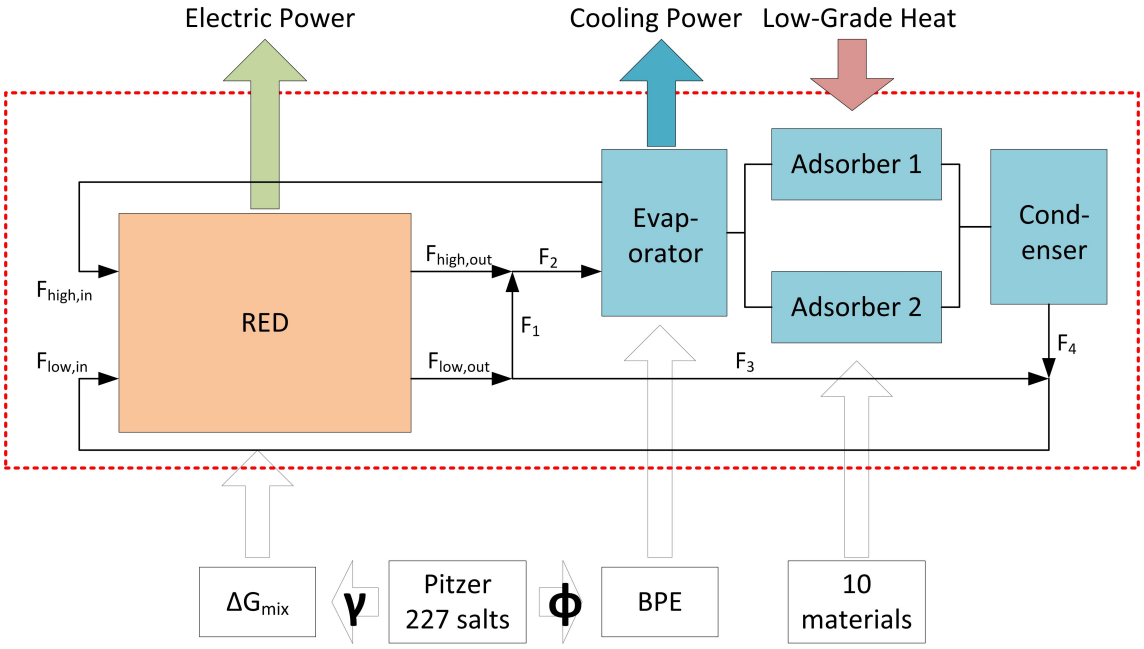

Figure 2: ADRED model illustrated in a simplified way

The entire system operates at the saturation pressures of the working fluid inside. Water vapour condensed at 30 °C necessitates an absolute condenser pressure of 0.04 bar [32]. However, the low pressure has no negative impact on the electricity generation, because RED is an electrochemical process driven by salinity gradients and not by pressure differences. In theory, the system could also be operated with different fluids and salt solutions. For example, the utilisation of solutions of pure liquid ammonia and salts would allow the operation of the system pressurised at an absolute pressure of 11.7 bar and a condenser temperature of 30 °C [32]. In addition, ammonia has a very low latent heat, which would increase evaporation and the efficiency of the regeneration. However, the mean activity coefficients of salt solutions with ammonia as solvent are low [33], which reduces ΔG_{mix}. Furthermore, RED membranes are designed for aqueous salt solutions, but not for ammonia or other solvents. Thus, water is the most feasible and environmentally friendly choice as fluid.

2.2. Modelling the ADRED system

The following assumptions were made for the model:

- Only salt ions pass through the RED membrane, but no water. This simplification is necessary to assess the electricity output by ΔG_{mix}. A salt specific membrane model would be required to evaluate the water transport through the membrane itself, which cannot be prevented in a real system. However, this investigation addresses the ideal case for a large number of salts, which is why the water transport through the membrane has been neglected.

- The electricity produced by the RED membrane is equal to the Gibbs free energy of mixing.
- The relationship between the activity of water and the saturation pressure is ideal.
- In most cases the specific heat capacity of the adsorption material $c_{p,AD}$ was not specified in the literature, so $c_{p,AD} \approx 1$ kJ/(kgK) was assuemed from [34].
- The mass of the heat exchangers was neglected for the analysis of the SEC as they already represent a system limitation and this analysis focuses on the ideal case.
- All the salt remains in the evaporator and only pure water vapour reaches the adsorption material.
- The cooling power is neglected as system output, because it would reduce the desalination capacity of the material. Cooling power and electricity production are a trade-off, where the negligence of cooling maximises the working capacity of the adsorption material and with it, the electricity production of the system.
- The study neglects the change of latent heat caused by the salt. The latent heat of the salt solution would affect the cooling power of the system, but the SEC is independent of the latent heat in the evaporator. The salt remains in the evaporator and affects the latent heat of the salt solution in the evaporator alone. This changes the cooling power output of the evaporator, which is neglected by the investigation. Only pure water vapour is assumed to reach the adsorption material, which is why the latent heat of pure water applies to adsorption and desorption of the pure water vapour. Thus, the enthalpy difference of the salt solution can be neglected, because it does not affect the adsorption material.
- The internal electricity consumption of the system was neglected to assess the maximum thermodynamic efficiency achievable with the system. However, this assumption is challenged with additional considerations following the main investigation to assess the impact on a real system application.
- For simplification the low and high salinity feed solutions to the RED stack have the same flow rate [12]

2.3. Model equations for the ADRED flow scheme

Fig. 2 also presents the set-up of the ADRED model. The discription in greyscale illustrates the base of the model with the Pitzer equations and the Dubinin Astakhov data for the adsorption materials, which are all required to assess the main part of the model highlighted by the dashed line. The Pitzer correlations provide the osmotic coefficient Φ and the activity coefficient γ for each of the 227 salts [35] at the desired concentration. The coefficient γ is needed to calculate ΔG_{mix} and thereby the electricity output of the RED membrane. The osmotic coefficient Φ is used to determine the boiling point elevation (BPE) of the high salinity solution. The high salinity solution is regenerated in the evaporator and its BPE influences the evaporator pressure $P_{sat}(T_{evap})$. The Dubinin Astakhov (DA) isotherm data for 10 adsorption materials was obtained from the literature [36–42]. The isotherms are needed to assess the energy required to regenerate the salt solutions. Salt balances based on the flow scheme in Fig. 2 determine the

amount of condensate needed to restore the salt gradient.

The mass and salt balances for the flow scheme in Fig. 2 are listed below.
Mass balances:

$$F_{High,in} = F_{Low,in} \tag{1}$$

$$F_1 = F_4 \tag{2}$$

$$F_{High,out} + F_1 = F_2 \tag{3}$$

$$F_{Low,out} - F_1 = F_3 \tag{4}$$

Salt balances:

$$F_{Low,out}C_{Low,out} + F_{High,out}C_{High,out} = F_{Low,in}C_{Low,in} + F_{High,in}C_{High,in} \tag{5}$$

$$F_2C_2 = F_{High,out}C_{High,out} + F_1C_1 \tag{6}$$

$$F_3C_{Low,out} = F_{low,in}C_{low,in} \tag{7}$$

$$C_{High,out} - C_{Low,out} = (1 - X)\ (C_{High,in} - C_{Low,in}) \tag{8}$$

F_i [kg/s] represents the flow rates and C_i [mol/kg] the salt concentrations. The conversion factor X determines the change of the salt concentrations after passing through the RED membrane. F_1 compensates for the amount of distillate F_4 to restore the initial salt concentrations $C_{high,in}$ and $C_{low,in}$.

2.4. Parameters calculated using Pitzer equations

The dimensionless osmotic coefficient Φ can be calculated using the following equation [35]:

$$\Phi - 1 = |z_M z_X| f^{\Phi} + m\left(\frac{2v_X v_M}{v}\right) B^{\Phi}_{MX} + m^2\left(\frac{2(v_M v_X)^{3/2}}{v}\right) C^{\Phi}_{MX} \tag{9}$$

Where z_M and z_X are the charges of the ions [-], while v_M and v_X are the number of ions [-]. The molality is given by m [mol/kg] and the other coefficients are as follows:

$$f^{\Phi} = -A_{\Phi}\left(\frac{I^{1/2}}{1 + bI^{1/2}}\right) \tag{10}$$

$$B^{\Phi}_{MX} = \beta^{(0)}_{MX} + \beta^{(1)}_{MX}\ e^{-\alpha I^{1/2}} \tag{11}$$

$$I = \frac{1}{2}\sum m_i z_i^2 \tag{12}$$

The coefficients b and α are constants with the values of 1.2 and 2 for all solutes [35]. The ionic strength is represented by I [mol/kg] in the equations above. For each salt, the viral coefficients $\beta_{MX}{}^{(0)}$, $\beta_{MX}{}^{(1)}$ and $C_{MX}{}^{\Phi}$ are given by Pitzer and Mayorga [35]. The Debye Hückel coefficient A_{Φ} for water is given by [35, 43]:

$$A_{\Phi} = \frac{1}{3}\left(\frac{2\pi N_0 \rho_w}{1000}\right)^{1/2}\left(\frac{e^2}{DkT}\right)^{3/2} \tag{13}$$

In eq. (13) N_0 represents the Avogadro constant [mol^{-1}], k is the Boltzmann constant [$m^2kg\ s^{-2}K$], e is the electron charge [C] and D the dielectric constant [-] [44]:

$$D = D_{1000} + C\ ln\left(\frac{B+P}{B+1000}\right) \tag{14}$$

where P is the saturation pressure of water at the corresponding temperature T [K]. The coefficients $U_{1\text{-}9}$ are shown in table 1.

$$D_{1000} = U_1\ exp(U_2T + U_3T^2) \tag{15}$$

$$C = U_4 + \frac{U_5}{U_6 + T} \tag{16}$$

$$B = U_7 + \frac{U_8}{T} + U_9T \tag{17}$$

Table 1: Coefficients used to calculate the dielectric constant of water [44]

U_1	342.8	U_6	−182.9
U_2	$-5.09 \cdot 10^{-3}$	U_7	−8032.5
U_3	$9.47 \cdot 10^{-7}$	U_8	$4.21 \cdot 10^{6}$
U_4	−2.05	U_9	2.14
U_5	3115.9		

The osmotic coefficient Φ [-] correlates with the water activity of the solution a_s [-] [45]:

$$\Phi = -\left(\frac{1000}{(v_M + v_X)mM}\right)ln(a_s) \tag{18}$$

where M is the molar mass [g/mol] of the solvent. The activity of the solution is used to assess the saturation pressure of the salt solution, which is needed to evaluate the pressure in the evaporator of the adsorption desalinator during adsorption. The relationship between the activity of the solution a_s, saturation pressure of water p_{sat,H_2O} [bar] and saturation pressure of the salt solution $p_{sat,sol}$ [bar] is:.

$$a_s = \frac{p_{sat,sol}}{p_{sat,H_2O}} \tag{19}$$

All saturation pressures were calculated by using NIST Refprop [46]. The Gibbs free energy of mixing represents a theoretical maximum value of the energy released due to the mixing of two

solutions in a reversible process. In reality, the mixing of solutions is an irreversible process, which increases the entropy of the solution. The useable energy is therefore lower than the Gibbs free energy of mixing [27], whereas the model evaluates the ideal case.
The Gibbs free energy of mixing per mole of mixture is defined as [27]:

$$-\Delta G_{mix} = RT\left\{\left[\sum x_i ln(\gamma_i x_i)\right]_M - \Lambda_A\left[\sum x_i ln(\gamma_i x_i)\right]_A - \Lambda_B\left[\sum x_i ln(\gamma_i x_i)\right]_B\right\} \tag{20}$$

where x_i are the mole fractions and Λ_A, Λ_B are the ratios of total moles of each solution based on the entire system $\Lambda_A + \Lambda_B = 1$. The Gibbs free energy of mixing can be simplified for an aqueous solution of strong electrolytes and low salt concentrations [27]. At low concentrations, the mole fraction of water is approximately one and the activity coefficient of water is one as well making the contribution of water in eq. (20) negligible, which is why ΔG_{mix} can be approximated to [27]:

$$-\frac{\Delta G_{mix}}{vRT} \approx c_M\ ln(\gamma_{s,M} c_M) - \Psi c_{low}\ ln(\gamma_{s,low} c_{low}) - (1-\Psi) c_{high}\ ln(\gamma_{s,high} c_{high}) \tag{21}$$

where v represents the total number of ions dissociated into the solution from each electrolyte and $\Psi \approx V_{low}/(V_{low}+V_{high})$. Fig. 2 shows the case of two inlet streams and two outlet streams from the membrane. For the case presented in Fig. 2 the Gibbs free energy of mixing is:

$$\begin{aligned} -\frac{\Delta G_{mix}}{vRT} \approx \Psi\ & c_{low,out}\ ln(\gamma_{s,low,out} c_{low,out}) + (1-\Psi) c_{high,out}\ ln(\gamma_{s,high,out} c_{high,out}) \\ & -\Psi\ c_{low,in}\ ln(\gamma_{s,low,in} c_{low,in}) - (1-\Psi) c_{high,in}\ ln(\gamma_{s,high,in} c_{high,in}) \end{aligned} \tag{22}$$

The activity coefficient γ can be obtained from the Pitzer correlations [35]:

$$ln(\gamma) = |z_M z_X| f^\gamma + m\left(\frac{2 v_X v_M}{v}\right) B^\gamma_{MX} + m^2\left(\frac{2(v_M v_X)^{3/2}}{v}\right) C^\gamma_{MX} \tag{23}$$

$$f^\gamma = -A_\Phi\left[\frac{I^{1/2}}{1+bI^{1/2}} + \frac{2}{b} ln(1+bI^{1/2})\right] \tag{24}$$

$$B^\gamma_{MX} = 2\beta^{(0)}_{MX} + \frac{2\beta^{(0)}_{MX}}{\alpha^2 I}\left[1 - e^{-\alpha I^{1/2}}(1 + \alpha I^{1/2} - (1/2)\alpha^2 I)\right] \tag{25}$$

$$C^\gamma_{MX} = \frac{3}{2} C^\Phi_{MX} \tag{26}$$

2.5. Energy and exergy performance based on an adsorption cycle analysis

During the regeneration the adsorber beds are heated and cooled as shown in the adsorption cycle in Fig. 3. The specific energy consumption is a performance parameter, which predicts the amount of energy required per kilogram of pure water desorbed [24]:

$$SEC = \frac{Q_{1\to2} + Q_{2\to3}}{M_{water}} \tag{27}$$

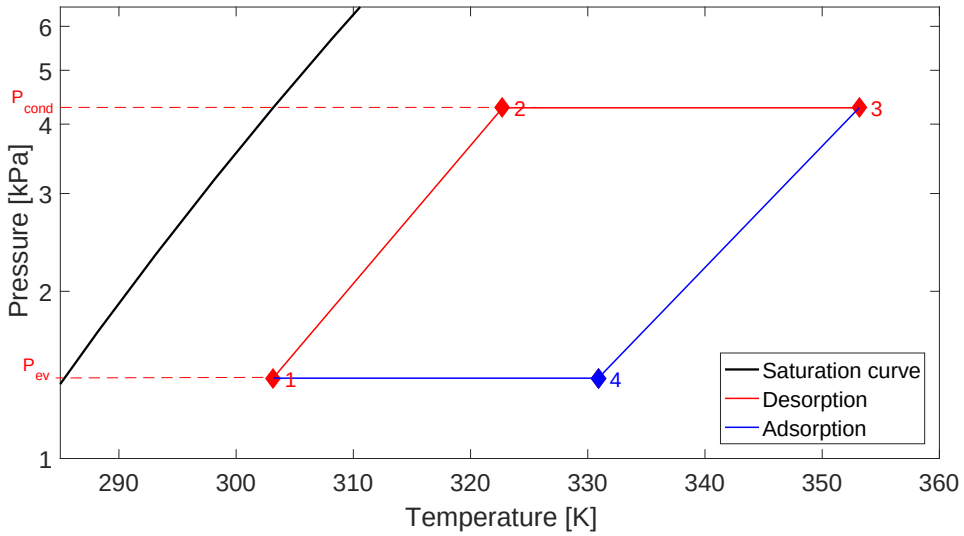

Figure 3: An exemplary graph representing an adsorption cycle. The cycle is split into desorption 1→3 and adsorption 3→1, where the first takes place during the heating phase (red) and the latter occurs during the cooling phase (blue) of the bed.

The SEC represents the energy $Q_{1\to2\to3}$ required for the desorption process, where the adsorption beds are heated by the low-grade heat source. The first contributor $Q_{1\to2}$ is the energy required for isosteric heating to increase the pressure from the saturation pressure of the evaporator to the saturation pressure of the condenser. Thus, the beds are heated from ambient temperature T_1 to the intermediate temperature T_2. During this the two valves connecting the adsorber to evaporator and condenser are closed to increase the pressure without any adsorption or desorption occurring during this step.

$$Q_{1\to2} = m_{AD}(W_1 C_{p,H_2O} + C_{p,AD}) \cdot (T_2 - T_1) \tag{28}$$

As soon as the pressure of the adsorber beds equals the pressure of the condenser, desorption begins. The valve between the adsorber and condenser is opened. As a result, water vapour desorbs from the material while the bed continues to be heated from the intermediate temperature T_2 to the temperature of the low-grade heat source T_3, which is both accounted for by $Q_{2\to3}$:

$$Q_{2\to3} = m_{AD}\left((T_2 - T_1) + \left[C_{p,AD} + \frac{W_2 + W_3}{2} C_{p,H_2O}\right] \cdot (T_3 - T_2) + (W_2 - W_3)\Delta h\right) \tag{29}$$

$$M_{water} = m_{AD}(W_2 - W_3) \tag{30}$$

$$SEC = \frac{(W_1 C_{p,H_2O} + C_{p,AD})(T_2 - T_1) + \left[C_{p,AD} + \frac{W_2+W_3}{2} C_{p,H_2O}\right](T_3 - T_2) + (W_2 - W_3)\Delta h}{W_2 - W_3} \tag{31}$$

The SEC [kJ/kg_{H_2O}] is assessed through the analysis of the thermodynamic cycles. This analy-

sis provides the parameters required in eq. (31), which are the temperatures at each state of the adsorption cycle i T_i [K], the uptake of the adsorption material W_i [kg/kg] and the operating pressures P_i [bar]. The mass of the adsorption material m_{AD} cancels out in the SEC equations and therefore does not need to be defined.

While the SEC is required for the energy analysis, it must be extended by the Carnot factor to perform an exergy analysis of the process. The Carnot factor in eq. (38) describes the theoretically highest possible efficiency between the boundaries of the ambient temperature T_{cond} and regeneration temperature T_{hot} [47].

$$\eta_c = 1 - \frac{T_{cond}}{T_{hot}} \tag{32}$$

At low temperatures only a small fraction of the energy provided to the system can be used by the process (exergy), which in this case is the energy content available between ambient temperature and the heat source temperature. The analysis of the exergy efficiency can be more useful than the energy efficiency alone, because it provides information on how well the available exergy is used by the process [47, 48].

$$\eta_{ex} = \frac{\eta}{\eta_c} \tag{33}$$

The exergetic SEC is defined in eq. (34):

$$SEC_{ex} = SEC\ \eta_c = \frac{(Q_{1\to2} + Q_{2\to3})\left(1 - \frac{T_a}{T_{hot}}\right)}{M_{water}} \tag{34}$$

In this study, the thermodynamic cycle was assessed by the use of the Dubinin-Astakhov isotherm (DA) [49].

$$W = W_0\ exp\left[-\left(\frac{A}{E}\right)^n\right] \tag{35}$$

$$A = -RT\ ln\left(\frac{P}{P_s}\right) \tag{36}$$

Where W_0 [kg/kg], E [kJ/kg] and n [-] are the Dubinin Astakhov parameters given in table 2. The isosteric heat of adsorption Δh was obtained from the following equation [50]:

$$\Delta h = L + E\ ln\left(\frac{W_0}{W}\right)^{1/n} + \frac{E\beta T}{n}\left(\frac{W_0}{W}\right)^{-(n-1)/n} \tag{37}$$

Where β is the coefficient of thermal expansion [1/K].

Table 2: Dubinin-Astakhov parameters for different materials with water. In the cases of 1*: $c_{p,AD}$ was not specified and $c_{p,AD}$ = 1 kJ/(kgK) was taken from [34].

Material	Type	W_0 [kg/kg]	E [kJ/kg]	n [-]	$c_{p,AD}$ [kJ/(kgK)]	Ref
Siogel	Silica Gel	0.38	220.0	1.10	0.8	[36]
Grace 127 B	Silica Gel	0.31	152.4	0.90	1*	[37]
Type-A5BW	Silica Gel	0.45	199.2	1.25	1*	[38]
Type-RD 2560	Silica Gel	0.33	243.6	1.35	1*	[38]
Type-A++	Silica Gel	0.49	211.3	1.35	1*	[38]
CPO-27(Ni)	MOF	0.46	556.3	4.00	1*	[39]
AQSOA Z01	Zeolite	0.21	222.2	5.00	1*	[40]
AQSOA Z02	Zeolite	0.31	388.9	3.00	1*	[40]
Köstrolith 13XBFK	Zeolite(13X)	0.34	1192.3	1.55	0.88	[41]
ZEOX OII	Zeolite(13X)	0.23	1266.7	1.20	1*	[42]

2.6. Integrating the SEC into the ADRED flow scheme

The SEC_{ex} expresses the exergy required to produce one kilogram of pure water. Thus, it needs to be integrated into the salt balances. In the model, both streams entering the RED membrane each have a mass flow of 1 kg/s and are mixed to a certain degree depending on the conversion factor X. The salt balances determine the amount of distillate F_4 that needs to be regenerated. Multiplying the SEC_{ex} with F_4 assesses the exergy needed to restore the salt concentrations in the model. The ratio of the key parameters indicates the exergy efficiency of the ADRED system.

$$\eta_{ex} = \frac{\Delta G_{mix}}{SEC\ \eta_c\ F_4} \tag{38}$$

3. Results and discussion

The ADRED model has eight degrees of freedom listed in table 3. In a preliminary investigation, the degrees of freedom were lowered to five to reduce the number of possible input scenarios from 20 million by two orders of magnitude. The aim was to calculate the exergetic performance for each combination of input scenarios and find the optimum combination of salt, material and system parameters.

Table 3: The degrees of freedom of the ADRED model

Parameter		**Unit**	**Range**	**No. of steps**
Evaporator Temperature	T_{evap}	[°C]	10-30	5
Condenser Temperature	T_{cond}	[°C]	20-30	3
Regeneration Temperature	T_{hot}	[°C]	60-100	5
Inlet concentration low	$C_{low,in}$	[mol/kg]	0-C_{max}	5
Inlet concentration high	$C_{high,in}$	[mol/kg]	C_{max}	1
Conversion factor	X	-	0.2-1	5
Salts	-	-	227	227
Adsorption materials	-	-	10	10

The preliminary investigation showed that the ratio of ΔG_{mix} to SEC_{ex} was highest at the maximum inlet concentration $C_{high,in}$ for all salts. The Pitzer tables [35] provide the maximum value of $C_{high,in}$=C_{max} for each salt and it was used for the analysis. Furthermore, an analysis of the SEC for the regeneration side was performed to choose the best temperatures for the evaporator and condenser T_{evap} and T_{cond}.

3.1. Temperature impact of the adsorption regeneration on the SEC

Twelve different, temperature combinations were identified to find the best temperature combination of T_{evap} and T_{cond} for the lowest SEC. For each combination, the exergetic SEC_{ex} was calculated for an aqueous 5 mol/kg NaCl solution in the evaporator, the ten adsorption materials and five different regeneration temperatures between 60-100 °C. Afterwards an SEC_{ex} was formed averaging all results for the regeneration temperatures taking all combinations of T_{evap} and T_{cond} into account as shown by the red bars in Fig. 4. The analysis of the total value for the SEC_{ex} ensures that the chosen temperature combination provides the best overall results for all the materials. In desalination T_{evap} and T_{cond} are usually equal [24]. The result in Fig. 4 is in accordance with the literature and T_{evap}=T_{cond}= 30 °C was selected as temperatures for the ADRED system simulation.

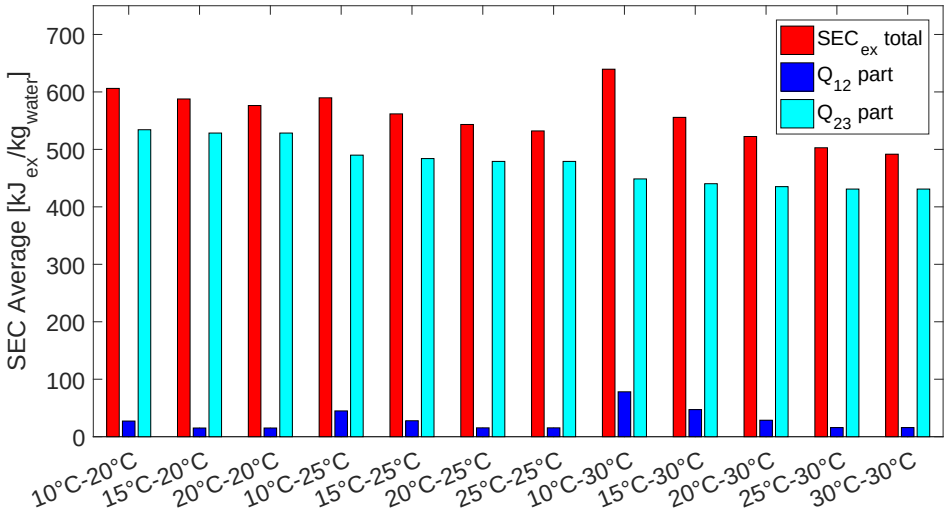

Figure 4: The average SEC_{ex} for each combination of T_{evap} to T_{cond}. Each bar represents the average value achieved after calculating all the SEC_{ex} for all materials and regeneration temperatures. Then, the SEC is split into its two main contributing parts as it can be seen in eq. (39). The concentration of NaCl in the evaporator is 5 mol/kg in this example.

In addition, the SEC_{ex} in Fig. 4 is split into the two parts $Q_{1\to2}$ and $Q_{2\to3}$ as shown in eq. (39).

$$SEC_{ex} = \frac{(Q_{1\to2})\left(1-\frac{T_{cond}}{T_{hot}}\right)\eta_c}{M_{water}} + \frac{(Q_{2\to3})\left(1-\frac{T_{cond}}{T_{hot}}\right)\eta_c}{M_{water}} \tag{39}$$

In Fig. 4, the difference of SEC_{ex} between the least and the most efficient temperature combination is almost 30 %, which is caused by the contribution of the isosteric heating $Q_{1\to2}$. The larger the pressure difference between evaporator and condenser, the more energy is needed to increase the pressure of the adsorption bed from the evaporator pressure to the condenser pressure. The first part of eq. (39) accounts for this, which can be seen in Fig. 4. The second part

of eq. (39) remains constant in Fig. 4 for each T_{cond}, even though the energy $Q_{2\to3}$ decreases at large temperature difference between T_{evap} and T_{cond} as it can be seen in Fig. 5. The amount of pure water M_{water} produced in each cycle decreases with the temperature difference as well. The two effects cancel each other out, which is why the second part of eq. (39) remains essentially constant in Fig. 4.

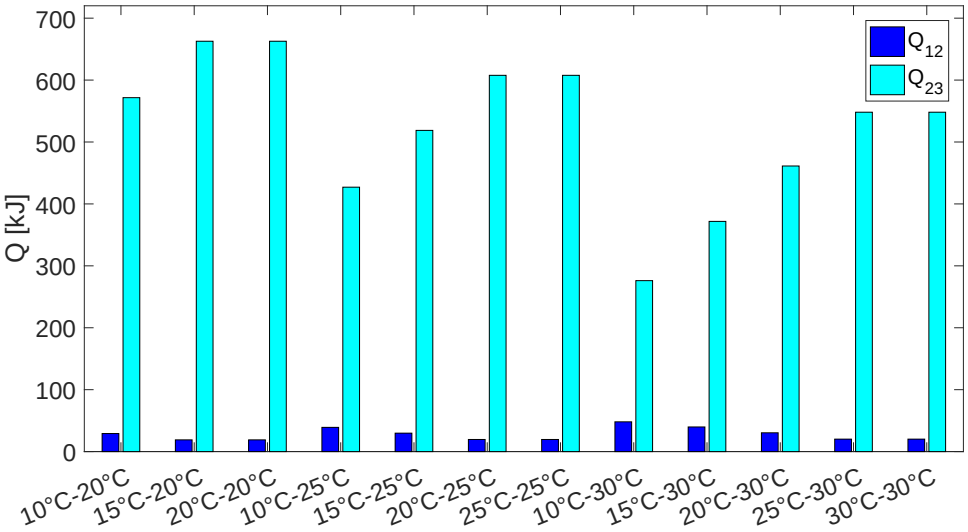

Figure 5: The average energy contribution of Q_{12} and Q_{23} for each combination of T_{evap} to T_{cond}. The concentration of NaCl in the evaporator is 5 mol/kg in this example

3.2. Influence of the boiling point elevation (BPE) on the adsorption cycle

Wu et al. [24] investigated the impact of the three temperature levels T_{evap}, T_{cond} and T_{hot} on the thermodynamic cycle in desalination, where they described the three possible cases $T_{evap} < T_{cond}$, $T_{evap} = T_{cond}$ and $T_{evap} > T_{cond}$. The results showed that the SEC for the case $T_{evap} \geq T_{cond}$ is generally the best.However Wu et al. neglected the presence of salt in the evaporator. The salt-free case they assumed for $T_{evap} = T_{cond}$ is shown in Fig. 6. In this case the thermodynamic cycle is reduced to a straight line, where the condenser and evaporator operate at the same pressure $P_{evap} = P_{cond}$. Hence the uptake $W_1 = W_{sat}$ is maximal and the process has the highest working capacity ΔW possible. By contrast, the second cycle shown in Fig. 6 illustrates the thermodynamic cycle of a 5 mol/kg MgI_2 solution considering the boiling point elevation, which reduces the pressure in the evaporator.

The BPE is defined as:

$$BPE = T_{sat,sol}(P_{sol}) - T_{sat,H_2O}(P_{sol}) \tag{40}$$

The effect of the BPE on the thermodynamic cycle in Fig. 6 is significant. The evaporator temperature in both cases in Fig. 6 remains the same $T_{evap} = 30$ °C. However, the BPE of 17 °C in the case of the MgI_2 solution lowers the pressure in the evaporator from 4.3 kPa to 1.4 kPa. As a result, the thermodynamic adsorption cycle of the aqueous MgI_2 solution in Fig. 6 has the same shape a pure water cycle would have of a pure water cycle at $T_{evap} = 13$ °C, $T_{cond} = 30$ °C and $T_{hot} = 80$ °C, even though the evaporator and condenser are actually operating at the same temperature $T_{evap} = T_{cond} = 30$ °C. This has significant impact on the water uptake of the material during adsorption ΔW, which is 19 % below the uptake in the salt-free case and

leads to a decreased water production per cycle by the same factor. Despite the reduced working capacity, the increase of the SEC by 4 % in the example is rather low, because a reduced working capacity requires a reduced amount of heat for desorption.

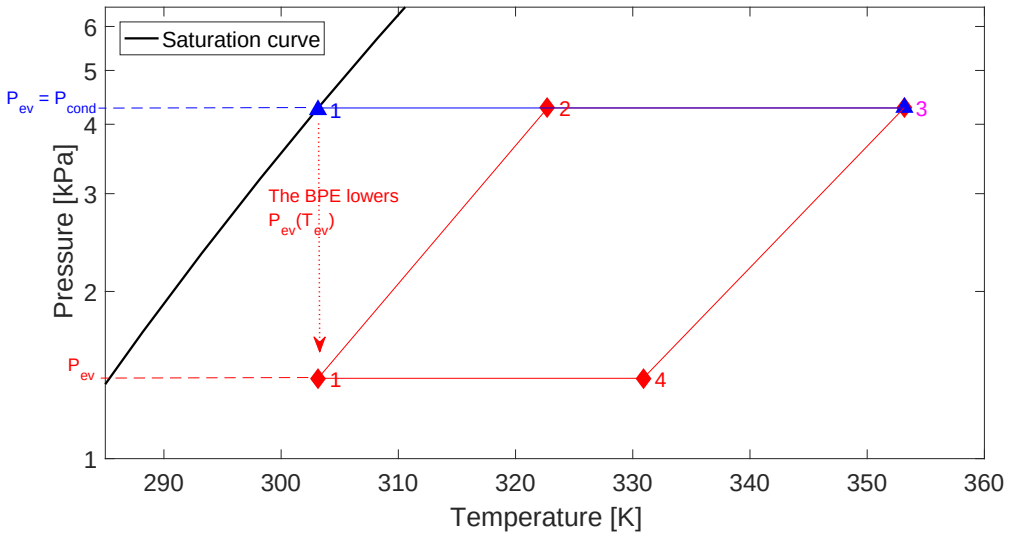

Figure 6: The boiling point elevation changes the shape of the thermodynamic cycle of AQSOA Z01. The blue line shows the cycle for pure water, while for the red line the boiling point elevation lowers the evaporator pressure. The temperatures in both cases are: $T_{evap} = T_{cond} = 30$ °C and $T_{hot} = 80$ °C. Salt concentration of MgI_2: △ 0 mol/kg, ◇ 5 mol/kg

Fig. 7 shows the change of the energetic SEC for two different example salts. Sodium chloride is an example of a monovalent salt while magnesium iodide represents a divalent salt. The influence of the concentration of NaCl on the SEC is 0.3 % in the range between 0-5 mol/kg, while the increase of the SEC of aqueous MgI_2 solutions is less than 4 % within the same concentration range as mentioned above. Hence, the influence of salt, concentration and BPE on the SEC are almost negligible.

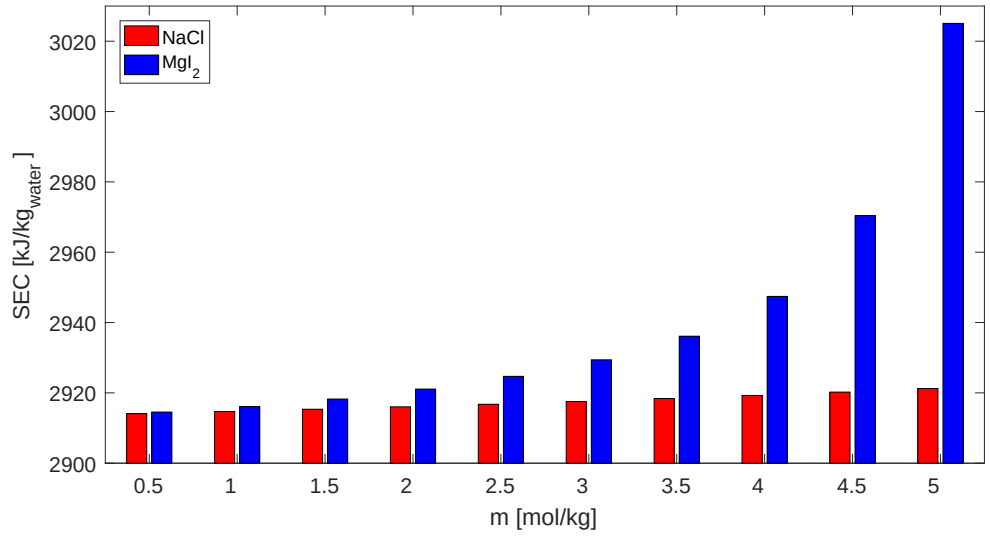

Figure 7: The influence of salts and their concentration are almost negligible for the energetic SEC of the adsorption regeneration

The independence between the salt concentration and the SEC is a very important aspect of the ADRED system. It allows the RED membrane to operate at optimal conditions without restrictions from the regeneration side. Thus, even saturation concentrations can be utilised in the ADRED system without lowering the specific performance of the adsorption regeneration.

3.3. Performance of the ADRED system

Fig. 8 shows the 15 best results of the ADRED system in terms of exergy and energy efficiencies and the corresponding input parameters. The results show that there is a possible range of low inlet concentrations $C_{low,in}$ between 0-2 mol/kg, which achieve a high performance. One could assume that a maximum salt gradient between the two inlet solutions would lead to the highest ΔG_{mix}. Nonetheless, the activity coefficients of the salts often have a minimum between zero and the maximum concentration. Hence a smaller salt gradient between the two inlet streams does not necessarily lead to a smaller ΔG_{mix}. In case of MgI_2 this minimum implies that the best efficiencies can be achieved at $C_{low,in}$=2 mol/kg.

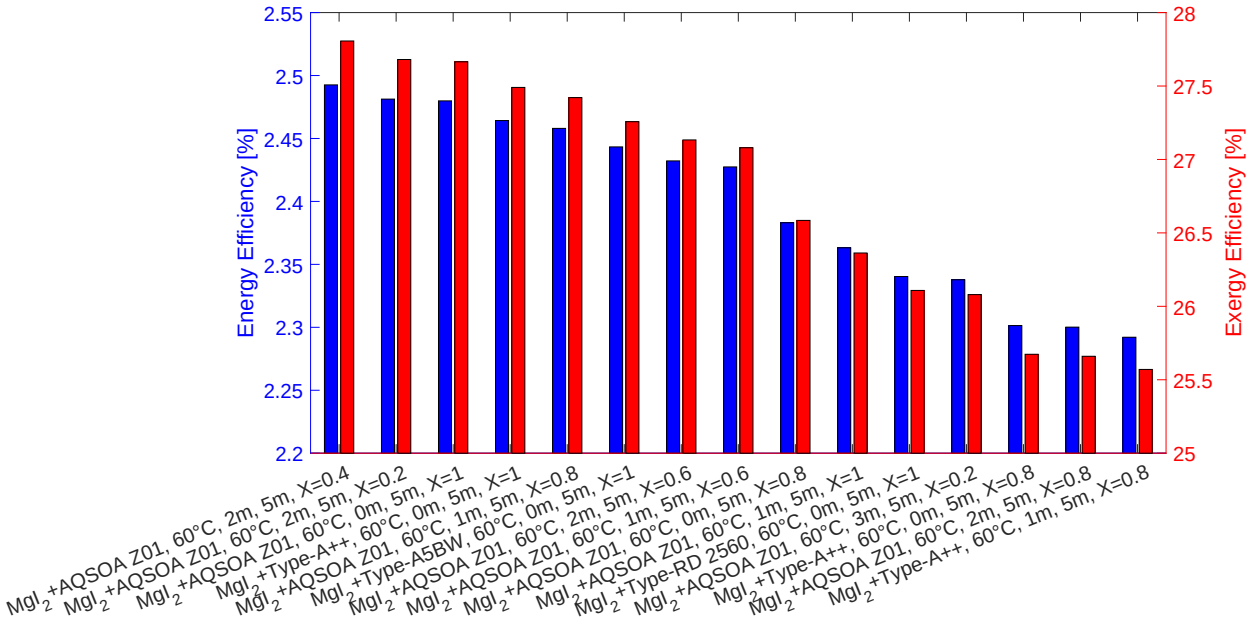

Figure 8: The 15 best results out of all 300,000 input scenarios. The blue bars represent the energy efficiencies and the red bars the exergy efficiencies

Looking at the conversion factor X in Fig. 8, the efficiency seems relatively independent of this parameter. A smaller value for X results in a smaller change of the salt gradient between the high and low salinity solutions after flowing through the membrane. As a result, less distillate needs to be produced during the regeneration to restore the initial salt gradient, therefore less energy is required for the regeneration. Conversely, less electricity is produced in the RED membrane because of the lower degree of mixing imposed by the conversion factor X. Both effects compensate for each other resulting in similar exergy efficiencies.

The best combination of salt and material is magnesium iodide and AQSOA Z01. Mitsubishi

AQSOA Z01 is an iron aluminophosphate with a pore diameter of 7.4 Å and the material exhibits a S-shaped isotherm which can be classified as Type IV/V [38, 40]. Kayel et al. [40] found that AQSOA Z01 is particularly suitable for the application in water adsorption chillers operating at regeneration temperatures below 65 °C.
The isotherms of AQSOA Z01 and Siogel silica gel are shown in Fig. 9. T_{evap} and T_{cond} are both 30 °C, which is why the pressures of evaporator and condenser should be equal. However, the presence of salt in the evaporator reduces the pressure due to the BPE. An exemple BPE of 10 °C is shown in Fig. 9. It can be seen that the uptake of the silica gel is reduced due to the BPE. However, the working capacity of AQSOA Z01 is less sensitive to a reduced P_{evap} due to its Type IV/V isotherm. Whereas, the working capacity of the silica gel decreases with increasing salt concentrations. Apart from the working capacity, the heat of adsorption Δh is a function of the uptake as well, but Δh of the two material types is very similar [51].

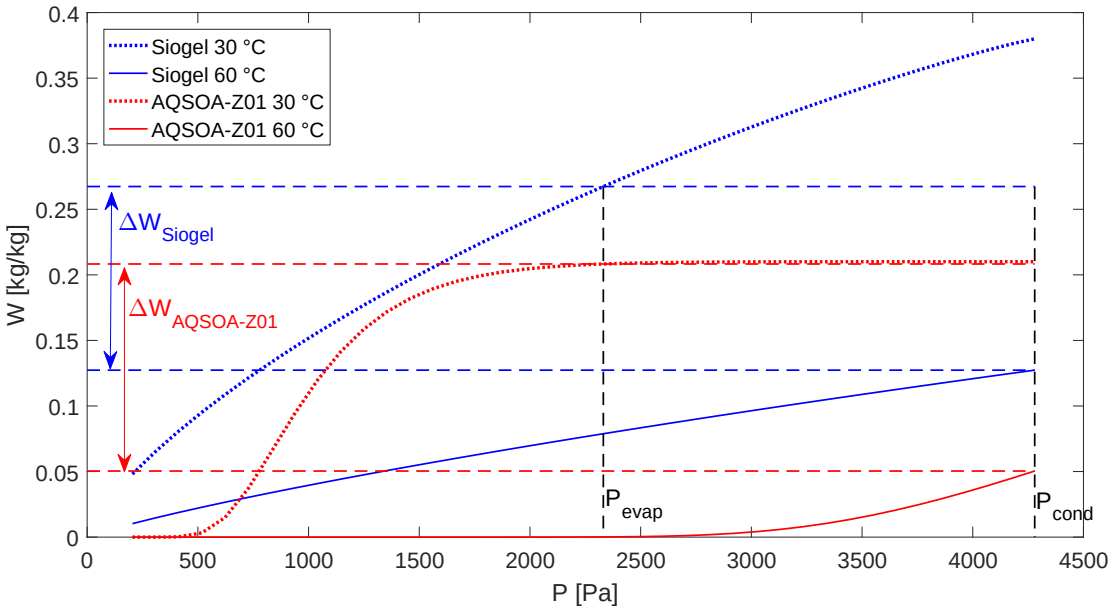

Figure 9: The working capacities ΔW resulting from the isotherms of an exemplary silica gel (Siogel) and AQSOA Z01 at $T_{evap} = T_{cond} = 30$ °C and a regeneration temperature of 60 °C. $P_{evap} \neq P_{cond}$ because BPE = 10 °C.

The overall performance of the silica gel is similar to the performance of AQSOA Z01. In addition to their good performance, silica gels are much cheaper than AQSOA Z01. Therefore, the combination of low-cost and performance makes silica gels very attractive materials for the application in the ADRED process.

Fig. 10 presents the best exergy efficiency achievable with each one of the materials. In addition, two cases were analysed, where one was for all salts and the other only for the monovalent salts. Two distinct cases were analysed because existing RED membranes are not designed for divalent salts and do not work very well with them [52]. Magnesium iodide gave the best results considering all materials and lithium chloride was the best monovalent salt. The high inlet concentrations for both salts were 5 mol/kg in the analysis. On average, the results for the monovalent LiCl were lower by a factor of 2.8 compared to the divalent MgI_2. LiCl is a

monovalent salt, which it why it works with existing membranes. At 5 mol/kg it can achieve an exergy efficiency of almost 10 % in an ADRED system.

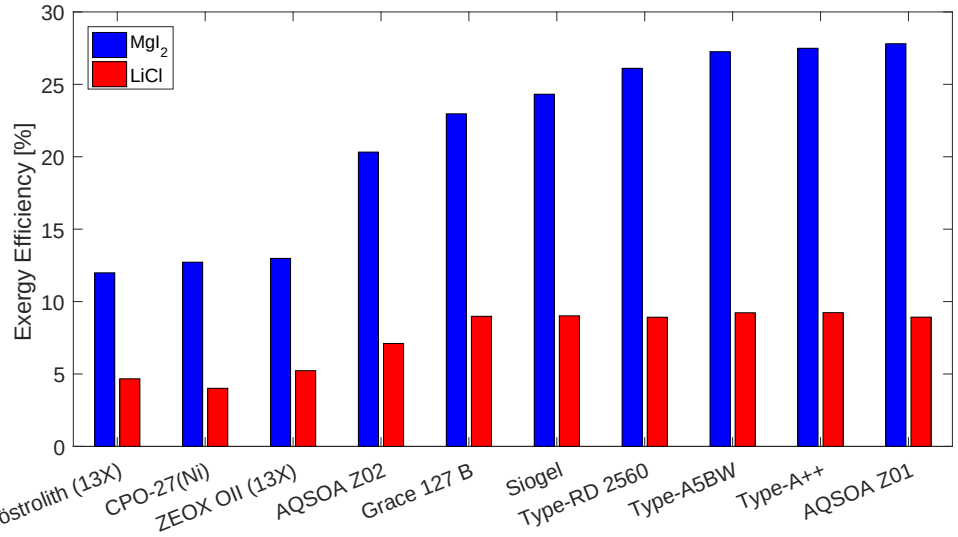

Figure 10: The best exergy performance scenarios for each material. The blue bars represent the best overall result for each material, all input scenarios and all salts, where MgI_2 is the best salt. The red bars are showing a second investigation where only monovalent salts were considered and LiCl is the best performing monovalent salt. The parameters used to achieve each result are listed in table 4.

The materials in Fig. 10 can be separated into two categories those that regenerate well at low temperatures and those that do not. The silica gels and AQSOA Z01 form the first category can be considered for the application in the ADRED system. By contrast, zeolite 13X, the metal organic framework and AQSOA Z02 require higher regeneration temperatures than considered in this study and therefore yield lower efficiencies.

Table 4: The overview of the parameters required to achieve the results shown in Fig. 10.

Material	**Type**	**Salt**	$\mathbf{T_{hot}}$ [°C]	$\mathbf{C_{low,in}}$ [mol/kg]	$\mathbf{C_{high,in}}$ [mol/kg]	**X** [-]
Siogel	Silica Gel	MgI_2	60	2	5	0.4
Grace 127 B	Silica Gel	MgI_2	60	2	5	0.4
Type-A5BW	Silica Gel	MgI_2	60	0	5	1
Type-RD 2560	Silica Gel	MgI_2	60	0	5	1
Type-A++	Silica Gel	MgI_2	60	0	5	1
CPO-27(Ni)	MOF	MgI_2	80	2	5	0.4
AQSOA Z01	Zeolite	MgI_2	60	2	5	0.4
AQSOA Z02	Zeolite	MgI_2	60	2	5	0.4
Köstrolith (13X)	Zeolite	MgI_2	60	0	5	1
ZEOX OII (13X)	Zeolite	MgI_2	60	0	5	1
all (excl. MOF)		LiCl	60	0	6	1
CPO-27(Ni)	MOF	LiCl	80	0	6	1

3.4. Impact of the process parameters on the exergy efficiency

Each of the key parameters T_{hot}, $C_{high,in}$, $C_{low,in}$ and the conversion factor X has a different leverage effect on the exergy efficiency. Fig. 11 shows the effect of each of the parameters

on the exergy efficiency of the ADRED model. For this analysis AQSOA Z01 was chosen as material and MgI_2 as best performing salt. The interactions of two variables were studied for four different cases as shown in Fig. 11.

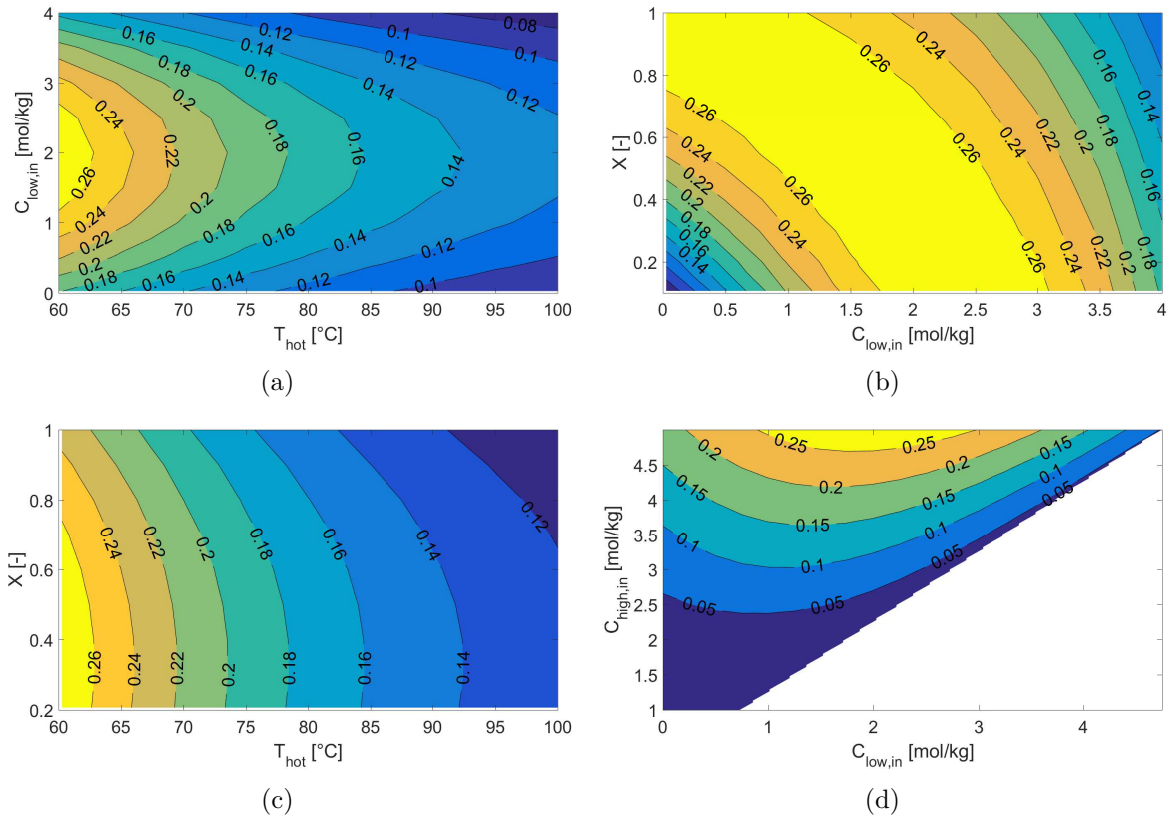

Figure 11: The exergy efficiencies on the contour lines are presented in absolute values.
(a) Exergy efficiency (MgI_2+AQSOA-Z01), where T_{hot} and $C_{low,in}$ are varied and X=0.4 and $C_{high,in}$=5 mol/kg remain constant.
(b) Exergy efficiency (MgI_2+AQSOA-Z01), where and $C_{low,in}$ and X are varied and T_{hot}=60 °C and $C_{high,in}$=5 mol/kg remain constant.
(c) Exergy efficiency (MgI_2+AQSOA-Z01), where T_{hot} and X are varied and $C_{low,in}$=2 mol/kg and $C_{high,in}$=5 mol/kg remain constant.
(d) Exergy efficiency (MgI_2+AQSOA-Z01), where and $C_{low,in}$ and $C_{high,in}$ are varied and T_{hot}=60 °C and X=0.4 remain constant.

In Fig. 11, the regeneration temperature T_{hot} and the inlet concentration of the low salinity solution $C_{low,in}$ are varied, while X=0.4 and $C_{high,in}$ = 5 mol/kg remain constant. The exergy efficiency decreases at higher regeneration temperatures proportionally to the Carnot factor. The Carnot factor at T_{hot} = 100 °C is two times bigger than it is at T_{hot} = 60 °C. Therefore, the specific exergy consumption SEC_{ex} doubles from T_{hot} = 60 °C to T_{hot} = 100 °C. The increase of SEC_{ex} leads to a proportional decrease of the exergy efficiency of the entire closed-loop system. As the exergy efficiency in Fig. 11 is most significantly dependent on the Carnot factor, it can be concluded that the adsorption material is sufficiently regenerated at 60 °C. Thus, a further increase of the regeneration temperature does not have significant advantages in terms of desorption. Furthermore, the inlet concentration of the low salinity solution peaks at $C_{low,in}$ = 2 mol/kg. The peak is caused by the conversion factor of X=0.4. Fig. 11 also shows an analysis where both, the conversion factor and $C_{low,in}$, were changed. The surface plot has a

ridge starting at $C_{low,in}$ = 2 mol/kg for low conversion factors and ending at $C_{low,in}$ = 0 mol/kg at complete mixing X = 1 of the two inlet solutions. Therefore, it is important to choose the combination of $C_{low,in}$ and the conversion factor X carefully, because it has a large impact on the performance. Finally, the exergy efficiency has a maximum at the highest $C_{high,in}$, but it is also important to keep the concentration at $C_{low,in}$ = 2 mol/kg in this example, because of X = 0.4. The increase of the salt gradient at the conversion factor X=0.4 would lower the exergy efficiency.

It appears that $C_{high,in}$ has the highest impact on the exergy efficiency followed by $C_{low,in}$, T_{hot} and X and have the lowest impact. $C_{low,in}$ and X are however correlated and need to be selected with care. The regeneration side has a lower impact on the exergy efficiency than the membrane side, because the impact of T_{hot} is lower than the impact of the concentrations. This confirms that the SEC_{ex} is relatively independent of the salt and its concentration as indicated in Fig 7. Therefore, increasing the salt concentration $C_{high,in}$ is the most straightforward approach to maximise performance.

3.5. Maximising the performance with a saturated aqueous LiCl solution

The maximum concentration provided by the Pitzer tables is one of the advantages and limitations for this work at the same time. The Pitzer tables provide information on a large number of salts, which allows them to be all considered for the system. In addition, for many salts the maximum concentrations provided by Pitzer match their maximum solubility. For example, the tables provide a concentration limit for MgI_2 of 5 mol/kg, which is consistent with the maximum solubility of 5.3 mol/kg at ambient temperature [53]. However, some salts have much higher solubilities than the Pitzer tables suggest and a higher concentration leads to a higher ΔG_{mix}. Lithium chloride was previously identified as the best monovalent salt at a concentration of 5 mol/kg. LiCl has an aqueous solubility of 20 mol/kg at ambient temperature [54]. Therefore, an additional simulation was performed to assess the system's performance for a saturated LiCl solution at 20 mol/kg.

Robinson published experimentally obtained activity coefficients, osmotic coefficients and water activities of LiCl solutions at 25 °C up to 20 mol/kg [55]. The previously described ADRED model was changed to use Robinson's data instead of the Pitzer correlations. Furthermore, the equation of ΔG_{mix} had to be altered from eq. (21) to eq. (20), because the assumption of relatively low concentrations does not apply to the saturated LiCl solution. On the adsorption side, a preheater for the evaporator was added to the process, because of the very high BPE(20 mol/kg, 30°C) = 33 °C. Without the preheater the pressure in the evaporator would be too low, which reduces the performance. Hence, the evaporator temperature was increased to the regeneration temperature $T_{ev} = T_{hot}$ = 60 °C. The condenser continues to operate at ambient temperature T_{cond} = 30 °C in the simulation.

The results of the investigation are shown in table 5. The exergy performance of the system is 45 % and energy efficiency is 4 %, which is a significant increase compared to the results at low concentrations. The higher concentration of the LiCl solution from 5 mol/kg to 20 mol/kg increases the SEC of the adsorption regeneration only by 6.5 %, while the Gibbs free energy

of mixing increases by a factor of seven. Hence, ADRED has great potential at very high salt concentrations. In addition, the performance of the much cheaper Siogel silica gel is almost the same as the performance achieved with AQSOA Z01.

Table 5: The performance of the ADRED system at very high concentrations of LiCl with a zeolite (AQSOA Z01) and silica gel (Siogel) as material

Material	T_{evap} [°C]	T_{cond} [°C]	T_{hot} [°C]	m [mol/kg]	η[%]	η_{ex} [%]
AQSOA Z01	60	30	60	20	4.0	44.6
Siogel	60	30	60	20	3.9	43.2

3.6. From thermodynamic considerations to a real system application

The 45 % exergy efficiency achieved with highly concentrated LiCl solutions represents an ideal value, which cannot be achieved due to real system limitations. The main investigation solely considered the thermal power input, but the real system would require electrical input for the operation as well. The pumps of an ADRED system would consume most of the electric power supplied to the system. Thus, the following considerations have been applied to quantifying the efficiency losses due to pumping power. Ng et al. estimated the electricity consumption of an AD desalination plant at 1.38 kWh/m^3 ($\approx$ 5 kJ/kg) taking into account the valves and three water pumps, which are needed to supply the heat exchangers of evaporator, condenser and adsorbers with heating/cooling water [25]. Several studies have investigated the pumping power consumption of RED plants, the results vary depending on the membrane design. Post et al. approximated the pumping energy losses at 5 % for spacer-free membranes [56, 57]. Tamburini et al. reported the pumping losses here at 3-25 % [7], while spacer-filled channels lead to a power loss of 10-20 % [7]. In comparison to the RED plants presented in the literature, the pumping energy within the ADRED process would be slightly higher at high salt concentrations because of the viscosity increase. For example, the dynamic viscosity of a LiCl solution at 17 mol/kg is 10 mPa·s and at 12 mol/kg it is 5 mPa·s, both at 25 °C [58].

In Fig. 12, the analysis was extended to incorporate pumping losses for the best results, which are LiCl at 5 mol/kg and 20 mol/kg, as well as MgI_2 at 5 mol/kg. The electricity consumption of the RED side of the system was estimated at 10 % for the salt solutions of 5 mol/kg and 20 % for the 20 mol/kg solution of LiCl, because of the increased viscosity. In addition, 5 kJ/kg of electricity were deducted from ΔG_{mix} to account for the electricity demands of the adsorption desalination side of the system. The results in Fig. 12 show that pumping losses reduce the exergy efficiency to 33 % for LiCl at 20 mol/kg, 6 % for LiCl at 5 mol/kg and 24 % for MgI_2. The results highlight the system's feasibility even after considering the pumping losses, which are relatively low because there are few moving parts within the system. In theory, the system could be operated with as little as 5 pumps in total: The 3 supply pumps to the adsorption desalinator and a pump for each of the high and low salinity solutions. Heat integration by connecting the cooling water of the condenser to the evaporator would reduce the number of required pumps down to 4.

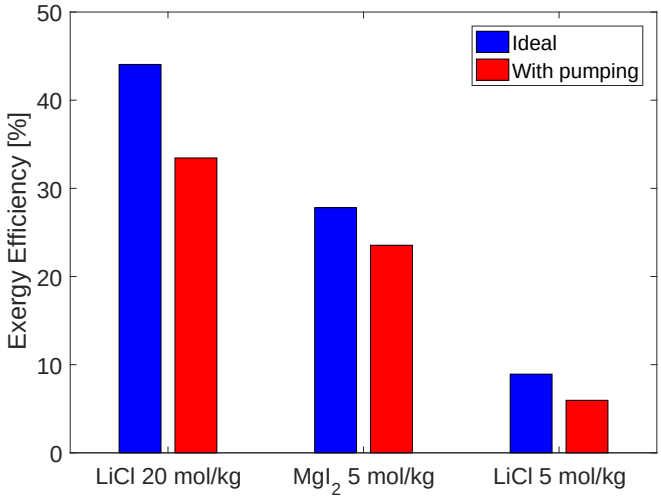

Figure 12: The results of the best performing salts with AQSOA Z01 with and without pumping losses

The main challenge for the implementation of the system remains on the membrane side. Permselectivity of existing RED membranes is reduced at high LiCl concentrations because of the small size of the Li ions. The reduced permselectivity causes a reduced membrane performance. Therefore, the exergy efficiency of 33 % including pumping losses still represents an ideal value, which demands improved membranes to be achievable.

This study demonstrates that ΔG_{mix} is large for Li-salts at very high concentrations, which can be provided by an AD desalinator. So far no other desalination technology connected in the closed-loop system to a RED membrane is able to supply such a high salinity solution to the RED stack. Thus, there was no incentive to develop such membranes. However, the energy requirements of the adsorption desalinator are independent of the salt concentration, which opens an entirely new field for the application of RED membranes in the future. A system operating at such high salt concentrations would face corrosion issues, where system components could be replaced by PEEK [26] and other polymers to prevent corrosion and lower the costs.

The size of the system is another contributor to the costs of the system. Currently, AD desalinators produce water at a Specific Daily Water Production of 10 m^3 per tonne of adsorption material per day [25]. This performance indicator multiplied by $\Delta G_{mix} \approx 93$ kJ/kg for LiCl at 20 mol/kg and subtracting pumping losses, results in a power output of 10.7 kW per tonne of adsorption material. Post et al. showed that a 200 kW RED plant could be mounted on a 40 ft sea container frame [56]. The electric output of 200 kW corresponds to the afore-mentioned paper plant emitting 6 MW of waste heat into the environment. The 200 kW RED plant would require 20 tonnes of silica gel, which corresponds to bed sizes of 7 m^3 each, if it is split among 4 adsorber beds. Thus, the adsorption plant would be small enough to be build inside another 40 ft sea container frame resulting in a footprint of 30 m^2 for the entire ADRED system.

4. Conclusion

In this study an entirely new process to generate electricity from low-grade waste heat using an Adsorption - Reverse Electrodialysis (ADRED) system has been developed. The ADRED system aims to generate electricity from low and high salinity solutions in a closed-loop system by utilising low-grade heat between 60-100 °C. After flowing through the Reverse Electrodialysis membrane the two solutions are regenerated by an adsorption desalinator driven by the low-grade heat source. Compared to other desalination methods, adsorption desalinators have a simpler system design, fewer moving parts, a lower electricity consumption and can utilise low-grade heat at 60 °C with current, commercially available materials. Future development of materials could reduce the regeneration temperature down to an unprecedented temperature of 40 °C.

A model for the prediction of exergy efficiencies for the ADRED system has been developed. The model has been used to screen 227 salts and ten different adsorption materials for their applicability in the ADRED system and calculate the exergy efficiency for each material, salt over a large number of possible system operating parameters.
A preliminary analysis was used to evaluate the impact of salts, their concentration and the resulting boiling point elevation on the specific exergy consumption of the adsorption regeneration. It was demonstrated that the specific exergy consumption is widely unaffected by the salt and its concentration. This is an important feature, because it allows the application of highly concentrated salt solutions and the optimisation of the Reverse Electrodialysis membrane without restrictions from the regeneration side. By contrast, other desalination methods impose constraints on the maximum salt concentration, because their thermal energy consumption increases with the salt concentration.

This investigation has focused on the performance of on the overall performance of the ADRED system. A total number of 300,000 different combinations of salts, materials and system parameters have been analysed to identify the optimum combination. Firstly, the study analysed the best overall results considering all salts. Secondly, the list of salts was reduced to monovalent salts, because current Reverse Electrodialysis membranes are designed for them. In the first analysis AQSOA Z01 proved to be an excellent material for low temperature regeneration, where it had the best performance and it performed best in combination with MgI_2 yielding an exergy efficiency of 28 %. In case of the monovalent salts, LiCl showed the highest performance. However, the Pitzer correlations are only fitted for LiCl up to a maximum concentration of 5 mol/kg, whereas the actual saturation concentration of this salt is 20 mol/kg. Therefore, an additional investigation assessed the performance with a saturated LiCl solution, as LiCl is the best monovalent salt from the main investigation. The result revealed an outstanding exergy efficiency of 45 % and an energy efficiency of 4 % with AQSOA Z01 as well as Siogel silica gel.

In a real system, the pumping losses would reduce the exergy efficiency of the system from 45 % down to 33 %. This system could convert the low-grade heat of a paper factory emitting 6 MW of hot exhaust air into 200 kW of electricity. An estimation of the system's footprint

demonstrated that the proposed 200 kW ADRED system would fit inside two 40 ft sea container frames. Another application could be the conversion of waste heat emitted by power plants amounting to 8500 TWh/year between 40-100 °C in the USA alone, which has a vast potential even at very low energy efficiencies. This illustrates the great capabilities of ADRED for the utilisation of low-grade heat.

Acknowledgements

The authors are grateful to Dr. Rhys Lloyd for his support during the preparation of the manuscript. This work was performed within the RED-Heat-to-Power project (Conversion of Low-grade Heat to Power through closed loop Reverse Electro-Dialysis) - Horizon 2020 programme, Project Number: 640667: `www.red-heat-to-power.eu`

Nomenclature

α	Constant
β	Coefficient of thermal expansion (1/K)
$\beta_{MX}^{(0)}$	Viral coefficient
$\beta_{MX}^{(1)}$	Viral coefficient
ΔG_{mix}	Gibbs free energy of mixing (kJ/kg)
Δh	Isosteric heat of adsorption (kJ/kg)
η	Thermal efficiency
η_c	Carnot efficiency factor
η_{ex}	Exergy efficiency
γ	Activity coefficient
Λ	Fraction of system's total moles
Φ	Osmotic coefficient
Ψ	Volumetric ratio
a_s	Activity of water
A_Φ	Debye Hückel coefficient
b	Constant
BPE	Boiling point elevation (K)
C_i	Salt concentrations (mol/kg)
c_p	Specific heat (kJ $kg^{-1}K^{-1}$)
C_{MX}^{Φ}	Viral coefficient
D	Dielectric constant
E	Dubinin-Astakhov parameter (kJ/kg)
e	Electron charge (C)
F_i	Salinity solution flow rates (kg/s)
I	Ionic strength (mol/kg)
k	Boltzmann constant ($m^2kg\ s^{-2}K$)
L	Latent heat (kJ/kg)
M	Molar mass (g/mol)
m_{AD}	Mass of silica gel (kg)
M_{water}	Mass of water produced in each cycle (kg)
N	Avogadro constant (mol^{-1})
n	Dubinin-Astakhov parameter
P	Pressure (bar)
R	Gas constant (J/mol K)
SEC	Specific energy consumption (kJ/kg)
SEC_{ex}	Specific exergy consumption (kJ/kg)
T	Temperature (K)
U_i	Dielectric constant parameters
v	Number of dissociated ions
W_i	Adsorption uptake (kg/kg)
X	Conversion factor
x	Mole fraction
z	Charge of ion

References

[1] Clemens Forman, Ibrahim Kolawole Muritala, Robert Pardemann, and Bernd Meyer. Estimating the global waste heat potential. *Renewable and Sustainable Energy Reviews*, 57:1568–1579, 2016.

[2] Mohammad Rahimi, Anthony P. Straub, Fang Zhang, Xiuping Zhu, Menachem Elimelech, Christopher A. Gorski, and Bruce E. Logan. Emerging electrochemical and membrane-based systems to convert low-grade heat to electricity. *Energy Environ. Sci.*, 11:276–285, 2018.

[3] Yasmine Ammar, Sharon Joyce, Rosemary Norman, Yaodong Wang, and Anthony P. Roskilly. Low grade thermal energy sources and uses from the process industry in the uk. *Applied Energy*, 89(1):3 – 20, 2012. Special issue on Thermal Energy Management in the Process Industries.

[4] Sarah Brückner, Selina Liu, Laia Miró, Michael Radspieler, Luisa F. Cabeza, and Eberhard Lävemann. Industrial waste heat recovery technologies: An economic analysis of heat transformation technologies. *Applied Energy*, 151:157 – 167, 2015.

[5] Michael Papapetrou, George Kosmadakis, Andrea Cipollina, Umberto La Commare, and Giorgio Micale. Industrial waste heat: Estimation of the technically available resource in the eu per industrial sector, temperature level and country. *Applied Thermal Engineering*, 138:207 – 216, 2018.

[6] Alexander S. Rattner and Srinivas Garimella. Energy harvesting, reuse and upgrade to reduce primary energy usage in the usa. *Energy*, 36(10):6172 – 6183, 2011.

[7] A. Tamburini, M. Tedesco, A. Cipollina, G. Micale, M. Ciofalo, M. Papapetrou, W. Van Baak, and A. Piacentino. Reverse electrodialysis heat engine for sustainable power production. *Applied Energy*, 206(Supplement C):1334 – 1353, 2017.

[8] Zhang Shengjun, Wang Huaixin, and Guo Tao. Performance comparison and parametric optimization of subcritical organic rankine cycle (orc) and transcritical power cycle system for low-temperature geothermal power generation. *Applied Energy*, 88(8):2740 – 2754, 2011.

[9] Francis J DiSalvo. Thermoelectric cooling and power generation. *Science*, 285(5428):703–706, 1999.

[10] Lon E Bell. Cooling, heating, generating power, and recovering waste heat with thermoelectric systems. *Science*, 321(5895):1457–1461, 2008.

[11] Evyatar Shaulsky, Chanhee Boo, Shihong Lin, and Menachem Elimelech. Membrane-based osmotic heat engine with organic solvent for enhanced power generation from low-grade heat. *Environmental science & technology*, 49(9):5820–5827, 2015.

[12] Michele Tedesco, Andrea Cipollina, Alessandro Tamburini, I. David L. Bogle, and Giorgio Micale. A simulation tool for analysis and design of reverse electrodialysis using concentrated brines. *Chemical Engineering Research and Design*, 93:441 – 456, 2015.

[13] Shihong Lin, Ngai Yin Yip, Tzahi Y Cath, Chinedum O Osuji, and Menachem Elimelech. Hybrid pressure retarded osmosis–membrane distillation system for power generation from low-grade heat: Thermodynamic analysis and energy efficiency. *Environmental science & technology*, 48(9):5306–5313, 2014.

[14] Gerald L. Wick. Power from salinity gradients. *Energy*, 3(1):95 – 100, 1978. Hydrogen in Metals Proceedings of the 2nd International Congress.

[15] J Veerman, M Saakes, SJ Metz, and GJ Harmsen. Reverse electrodialysis: performance of a stack with 50 cells on the mixing of sea and river water. *Journal of Membrane Science*, 327(1):136–144, 2009.

[16] Michele Tedesco, Claudio Scalici, Davide Vaccari, Andrea Cipollina, Alessandro Tamburini, and Giorgio Micale. Performance of the first reverse electrodialysis pilot plant for power production from saline waters and concentrated brines. *Journal of Membrane Science*, 500:33–45, 2016.

[17] David A. Vermaas, Damnearn Kunteng, Michel Saakes, and Kitty Nijmeijer. Fouling in reverse electrodialysis under natural conditions. *Water Research*, 47(3):1289 – 1298, 2013.

[18] Bruce E Logan and Menachem Elimelech. Membrane-based processes for sustainable power generation using water. *Nature*, 488(7411):313, 2012.

[19] Giorgio Micale, Andrea Cipollina, and Lucio Rizzuti. *Seawater Desalination for Freshwater Production*, pages 1–15. Springer Berlin Heidelberg, Berlin, Heidelberg, 2009.

[20] Patricia Palenzuela, Ashraf S. Hassan, Guillermo Zaragoza, and Diego-C. Alarcón-Padilla. Steady state model for multi-effect distillation case study: Plataforma solar de almería med pilot plant. *Desalination*, 337:31 – 42, 2014.

[21] Ali Al-Karaghouli and Lawrence L. Kazmerski. Energy consumption and water production cost of conventional and renewable-energy-powered desalination processes. *Renewable and Sustainable Energy Reviews*, 24(Supplement C):343 – 356, 2013.

[22] G. Zaragoza, A. Ruiz-Aguirre, and E. Guillén-Burrieza. Efficiency in the use of solar thermal energy of small membrane desalination systems for decentralized water production. *Applied Energy*, 130:491 – 499, 2014.

[23] G. Santori, A. Frazzica, A. Freni, M. Galieni, L. Bonaccorsi, F. Polonara, and G. Restuccia. Optimization and testing on an adsorption dishwasher. *Energy*, 50:170 – 176, 2013.

[24] Jun W Wu, Eric J Hu, and Mark J Biggs. Thermodynamic cycles of adsorption desalination system. *Applied energy*, 90(1):316–322, 2012.

[25] Kim Choon Ng, Kyaw Thu, Youngdeuk Kim, Anutosh Chakraborty, and Gary Amy. Adsorption desalination: an emerging low-cost thermal desalination method. *Desalination*, 308:161–179, 2013.

[26] C. Olkis, S. Brandani, and G. Santori. A small-scale adsorption desalinator. *Submitted to the 10th International Conference on Applied Energy ICAE 2018*, 2018.

[27] Ngai Yin Yip and Menachem Elimelech. Thermodynamic and energy efficiency analysis of power generation from natural salinity gradients by pressure retarded osmosis. *Environmental science & technology*, 46(9):5230–5239, 2012.

[28] Jan W. Post, Hubertus V. M. Hamelers, and Cees J. N. Buisman. Energy recovery from controlled mixing salt and fresh water with a reverse electrodialysis system. *Environmental Science & Technology*, 42(15):5785–5790, 2008. PMID: 18754509.

[29] Lingbo Kong, Lynn Price, Ali Hasanbeigi, Huanbin Liu, and Jigeng Li. Potential for reducing paper mill energy use and carbon dioxide emissions through plant-wide energy audits: A case study in china. *Applied Energy*, 102:1334 – 1342, 2013. Special Issue on Advances in sustainable biofuel production and use - XIX International Symposium on Alcohol Fuels - ISAF.

[30] Giulio Santori, Alessio Sapienza, and Angelo Freni. A dynamic multi-level model for adsorptive solar cooling. *Renewable Energy*, 43(Supplement C):301 – 312, 2012.

[31] Giulio Santori, Salvatore Santamaria, Alessio Sapienza, Stefano Brandani, and Angelo Freni. A stand-alone solar adsorption refrigerator for humanitarian aid. *Solar Energy*, 100(Supplement C):172 – 178, 2014.

[32] VDI Wärmeatlas. 10. auflage, 2006.

[33] WE Larsen and Herschel Hunt. Liquid ammonia as a solvent. iv. activities of ammonium nitrate, iodide, bromide, and chloride at 25° c. *The Journal of Physical Chemistry*, 39(6):877–884, 1935.

[34] Stefano Brandani, Celio Cavalcante, Anemir Guimarães, and Douglas Ruthven. Heat effects in zlc experiments. *Adsorption*, 4(3):275–285, Sep 1998.

[35] Kenneth S Pitzer and Guillermo Mayorga. Thermodynamics of electrolytes. ii. activity and osmotic coefficients for strong electrolytes with one or both ions univalent. *The Journal of Physical Chemistry*, 77(19):2300–2308, 1973.

[36] Alessio Sapienza, Andreas Velte, Ilya Girnik, Andrea Frazzica, Gerrit Füldner, Lena Schnabel, and Yuri Aristov. "water - silica siogel" working pair for adsorption chillers: Adsorption equilibrium and dynamics. *Renewable Energy*, 110(Supplement C):40 – 46, 2017.

[37] Douglas B Riffel, Ferdinand P Schmidt, Francisco A Belo, Antonio PF Leite, Farid B Cortés, Farid Chejne, and Felix Ziegler. Adsorption of water on grace silica gel 127b at low and high pressure. *Adsorption*, 17(6):977–984, 2011.

[38] Kyaw Thu, Anutosh Chakraborty, Bidyut Baran Saha, and Kim Choon Ng. Thermophysical properties of silica gel for adsorption desalination cycle. *Applied Thermal Engineering*, 50(2):1596–1602, 2013.

[39] Eman Elsayed, AL-Dadah Raya, Saad Mahmoud, Paul A Anderson, Ahmed Elsayed, and Peter G Youssef. Cpo-27 (ni), aluminium fumarate and mil-101 (cr) mof materials for adsorption water desalination. *Desalination*, 406:25–36, 2017.

[40] Sibnath Kayal, Sun Baichuan, and Bidyut Baran Saha. Adsorption characteristics of aqsoa zeolites and water for adsorption chillers. *International Journal of Heat and Mass Transfer*, 92:1120–1127, 2016.

[41] Barbara Mette, Henner Kerskes, Harald Drück, and Hans Müller-Steinhagen. Experimental and numerical investigations on the water vapor adsorption isotherms and kinetics of binderless zeolite 13x. *International Journal of Heat and Mass Transfer*, 71:555 – 561, 2014.

[42] Daniel Ferreira, Roberto Magalhaes, Pedro Taveira, and Adelio Mendes. Effective adsorption equilibrium isotherms and breakthroughs of water vapor and carbon dioxide on different adsorbents. *Industrial & Engineering Chemistry Research*, 50(17):10201–10210, 08 2011.

[43] Leonard F Silvester and Kenneth S Pitzer. Thermodynamics of electrolytes. 8. high-temperature properties, including enthalpy and heat capacity, with application to sodium chloride. *The Journal of Physical Chemistry*, 81(19):1822–1828, 1977.

[44] Daniel J Bradley and Kenneth S Pitzer. Thermodynamics of electrolytes. 12. dielectric properties of water and debye-hueckel parameters to 350. degree. c and 1 kbar. *Journal of physical chemistry*, 83(12):1599–1603, 1979.

[45] Bert R Staples and Ralph L Nuttall. The activity and osmotic coefficients of aqueous calcium chloride at 298.15 k. *Journal of Physical and Chemical Reference Data*, 6(2):385–408, 1977.

[46] Eric W. Lemmon, M. L. Huber, and M. O. McLinden. *NIST Standard Reference Database 23: Reference Fluid Thermodynamic and Transport Properties - REFPROP*. National Institute of Standards and Technology, Standard Reference Data Program, Gaithersburg, 9.0 edition, 2010.

[47] Peter Stephan, Karlheinz Schaber, Karl Stephan, and Franz Mayinger. *Thermodynamische Prozesse, Maschinen und Anlagen*, pages 319–397. Springer Berlin Heidelberg, Berlin, Heidelberg, 2013.

[48] Ibrahim Dincer and Marc A Rosen. *Exergy: energy, environment and sustainable development*. Newnes, 2012.

[49] M. M. Dubinin and V. A. Astakhov. Development of the concepts of volume filling of micropores in the adsorption of gases and vapors by microporous adsorbents. *Bulletin of the Academy of Sciences of the USSR, Division of chemical science*, 20(1):3–7, Jan 1971.

[50] Duong D Do. *Adsorption Analysis: Equilibria and Kinetics:(With CD Containing Computer Matlab Programs)*, volume 2. World Scientific, 1998.

[51] M.J. Goldsworthy. Measurements of water vapour sorption isotherms for rd silica gel, aqsoa-z01, aqsoa-z02, aqsoa-z05 and ceca zeolite 3a. *Microporous and Mesoporous Materials*, 196:59 – 67, 2014.

[52] Ramato Ashu Tufa, Sylwin Pawlowski, Joost Veerman, Karel Bouzek, Enrica Fontananova, Gianluca di Profio, Svetlozar Velizarov, João Goulão Crespo, Kitty Nijmeijer, and Efrem Curcio. Progress and prospects in reverse electrodialysis for salinity gradient energy conversion and storage. *Applied Energy*, 225:290 – 331, 2018.

[53] Sanjay R. Chemburkar. *Magnesium Iodide. e-EROS Encyclopedia of Reagents for Organic Synthesis*. John Wiley & Sons, Ltd, 2001.

[54] J.R. Rumble and J. Rumble. *CRC Handbook of Chemistry and Physics, 98th Edition*. CRC Handbook of Chemistry and Physics. CRC Press LLC, 2017.

[55] RA Robinson. The water activities of lithium chloride solutions up to high concentrations at 25°. *Transactions of the Faraday Society*, 41:756–758, 1945.

[56] J. W. Post, C. H. Goeting, J. Valk, S. Goinga, J. Veerman, H. V. M. Hamelers, and P. J. F. M. Hack. Towards implementation of reverse electrodialysis for power generation from salinity gradients. *Desalination and Water Treatment*, 16(1-3):182–193, 2010.

[57] Alexandros Daniilidis, Rien Herber, and David A. Vermaas. Upscale potential and financial feasibility of a reverse electrodialysis power plant. *Applied Energy*, 119:257 – 265, 2014.

[58] J Martin Wimby, Thore S Berntsson, et al. Viscosity and density of aqueous-solutions of libr, licl, znbr2, cacl2, and lino3. 1. single salt-solutions. *Journal of Chemical and Engineering Data*, 39(1):68–72, 1994.